Onset of erosion of a granular bed in a channel driven by fluid flow

Anyu Hong, Mingjiang Tao, and Arshad Kudrolli

Citation: Physics of Fluids (1994-present) **27**, 013301 (2015); doi: 10.1063/1.4905146
View online: http://dx.doi.org/10.1063/1.4905146
View Table of Contents: http://scitation.aip.org/content/aip/journal/pof2/27/1?ver=pdfcov
Published by the AIP Publishing

PHYSICS OF FLUIDS **27**, 013301 (2015)

Onset of erosion of a granular bed in a channel driven by fluid flow

Anyu Hong,[1,2] Mingjiang Tao,[3] and Arshad Kudrolli[2,a)]
[1]*College of Water Resources and Architectural Engineering, Northwest A&F University, Yangling, Shaanxi Province 712100, China*
[2]*Department of Physics, Clark University, Worcester, Massachusetts 01610, USA*
[3]*Department of Civil and Environmental Engineering, Worcester Polytechnic Institute, Worcester, Massachusetts 01609, USA*

(Received 17 September 2014; accepted 15 December 2014; published online 6 January 2015)

We investigate the erosion threshold of a granular bed driven by a fluid flow as a function of grain size and grain roughness. Experiments are performed with a bed in an enclosed cylindrical channel under laminar flow conditions. The shear rate at threshold for a prescribed flow rate is obtained from the height of the fluid above the bed as it comes to rest, and used along with the grain size to determine the particle Reynolds number Re_p. We estimate that the shear lift force acting on the granular surface is negligible over the range of Re_p investigated. We calculate the critical Shields number θ_c given by the ratio of the viscous shear stress and the normal gravitation and buoyancy stresses at the threshold of motion. We find that bed armoring leads to a systematic significant increase in θ_c independent of the grain roughness. This observed increase is of the same order of magnitude as scatter reported in the literature when θ_c is drawn from different data sets. While comparing similarly prepared beds with increasing particle size, we find that θ_c decreases systematically with Re_p, in contrast with the Shields curve which is constant at low Re_p. In order to understand the condition at erosion threshold, we use the condition of torque balance at threshold to determine the critical torque needed to dislodge grains due to viscous drag. This torque is found to be significantly lower than the value needed to dislodge a spherical grain on the bed surface which is fully exposed to a linear shear flow. However, further studies of the surface packing and its evolution are needed to fully understand the observed systematic dependence on the grain size and bed preparation. © *2015 AIP Publishing LLC.* [http://dx.doi.org/10.1063/1.4905146]

I. INTRODUCTION

The erosion threshold for a granular bed driven by a fluid flow is important in a number of natural processes and industrial applications. Examples include sediment transport in rivers, flow of particulates in subterranean fractures, turbidity currents, and slurries in pipelines and mixing tanks. A significant number of studies have been conducted on the threshold of erosion in rivers and flumes under laminar and turbulent flow conditions.[1–8] These studies often use the Shields number θ to characterize the relative magnitude of the shear stress and the normal stress acting on the granular bed due to the fluid flow. In the case where the bed is horizontal, and lift forces are negligible, the onset of erosion corresponds to the critical Shields number given by

$$\theta_c = \frac{\tau_c}{\sigma_g}, \tag{1}$$

a)Author to whom correspondence should be addressed. Electronic mail: akudrolli@clarku.edu

where τ_c is the critical shear stress due to fluid drag forces, and σ_g the normal stress given by the buoyancy corrected weight of a grain in the fluid.

It can be noted that τ_c depends on the Reynolds number Re of the fluid flow and the packing of the grains and roughness of the bed surface. While Re of the fluid flow is important to the transport of sediment, the viscous boundary layer near the bed surface is considered to be most relevant to the onset of erosion even in the case of turbulent flows, provided the particles are within the viscous boundary layer.[1] Therefore, a particle Reynolds number Re_p is defined by using the grain diameter d as the length scale and the slip velocity of the fluid near the granular interface v_s. Thus,

$$Re_p = \frac{\rho_f v_s d}{\mu}, \tag{2}$$

where ρ_f is the density of the fluid and μ the dynamic viscosity of the fluid. Because the fluid velocity is considered to be nearly zero inside the bed, v_s is often approximated as $\dot{\gamma} d$, where $\dot{\gamma}$ is the shear rate of the fluid near the bed. The curve which captures the overall trend of θ_c versus Re_p is often referred to as the Shields curve. However, Buffington and Montgomery[2] have noted that the reported data showed wide scatter (over an order of magnitude for a particular Re_p) when compiled from the published literature, which may result from the fact that the precise fluid flow and bed conditions were often unknown.

More recently, a number of laboratory based experiments have investigated the onset of erosion with idealized granular particles under laminar flow conditions. Charru *et al.*[9] studied the motion of monodisperse acrylic beads inside an annular channel in which the top plate was rotated at a prescribed rate to drive the fluid flow. They found significant armoring of the bed when it was sheared over prolonged periods due to consolidation of the bed, and further estimated θ_c to be 0.12 by assuming $\tau_c = \mu\dot{\gamma}$. By contrast, Lobkovsky *et al.*[12] measured the onset of erosion of glass beads in a channel with a uniform cross section and found $\theta_c \sim 0.3$. This value is considerably higher than those reported in other laboratory experiments performed at relatively low Re_p.[9–11] Thus, considerable variation in the reported θ_c can be noted even in the laboratory experiments which use similar estimates of shear stress and neglect lift forces.

Several theoretical and numerical studies have also examined the threshold for motion of a grain on a surface both at low and high Reynolds numbers.[13–16] A mathematical expression for the critical shear stress was derived by Wiberg and Smith[13] using force balance as the condition for stability at the granular surface and compared to the Shields curve. Numerical simulations by Derksen and Larsen[14] have shown that the drag and lift forces are further significantly affected by the surface coverage of the spheres in the top layer of the bed. More recently, Lee and Balachandar[16] have noted that the torque balance about a pivot point given by the angle of repose is the appropriate condition to consider the stability of a grain for the onset of erosion at the bed surface, which leads to a different condition than that using force balance especially at low Reynolds numbers.

Here, we discuss experiments to investigate the onset of granular erosion as a function of grain size, roughness, and fluid flow conditions in the laminar flow regime. We consider the magnitudes of drag, gravitational, and shear lift forces acting on a grain, and compare our results with a torque balance based stability criterion for a grain at the bed surface. We find significant armoring of the bed as it is sheared by the bed load. Further, we find that the critical Shields number decreases systematically with particle Reynolds number when varied by increasing the grain size. We show that this decreasing trend is observed in a regime where the critical Shields number is expected to be constant because the particle Reynolds number is much less than one.

II. EXPERIMENTAL SYSTEM

The experimental apparatus is similar to that used in a previous study[12] and consists of a transparent glass pipe with a rectangular cross section with length $L = 405$ mm, width $w = 26$ mm, and depth $b = 33$ mm as shown schematically in Fig. 1(a). This geometry was used because analytical expressions for the velocity profile and the shear stress acting on the boundaries are available for laminar flow. Granular materials with various grain sizes and roughness, used to investigate their

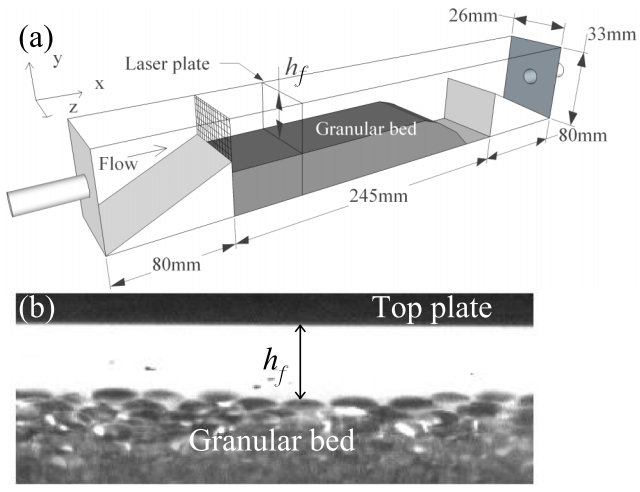

FIG. 1. (a) A schematic diagram of the experimental apparatus. (b) A sample image of the channel cross section used to extract the height of the fluid h_f above the granular bed. The grains corresponded to G-4 listed in Table I.

role on the onset of erosion, are listed in Table I. In particular, smooth glass beads with material density $\rho_g = 2.50\,\mathrm{g\ cm^{-3}}$ and rough quartz particles with $\rho_g = 2.65\,\mathrm{g\ cm^{-3}}$ are studied. A maximum angle of stability ϕ_m of the grains was measured by immersing the grains in a similar liquid and in a similar sized container and slowly tilting that container. The angle at which the grains are observed to move is recorded and averaged over five runs for each of the materials investigated. These averaged values of ϕ_m are reported for each of the materials in Table I. Figure 2 shows images obtained with a Scanning Electron Microscope (SEM) for the two different kinds of materials to give an idea of their surface roughness.

A water and glycerol mixture is used as the fluid with a bulk density $\rho_f = 1.23\ \mathrm{g\ cm^{-3}}$ and kinematic viscosity $\nu = 1.08 \times 10^{-4}\ \mathrm{m^2\ s^{-1}}$ at 20 °C. Such a viscous fluid is observed to give rise to laminar flow and is known to be Newtonian.[17] A fluorescent dye Rhodamine B is added to the fluid to visualize the fluid and to obtain the location of the granular surface. The fluid fills the entire channel and enters through a wire mesh as shown in the Fig. 1(a) and exits at the opposite end. The flow is generated by a peristaltic pump with a prescribed flow rate Q between 50 $\mathrm{cm^3\,min^{-1}}$ and 1000 $\mathrm{cm^3\,min^{-1}}$.

The bed is prepared by partially filling the channel with one of the granular materials listed in Table I. The bed surface is initialized before each experiment by first orienting the channel along the vertical direction, allowing the granular material to settle to the bottom, and then slowly tilting it back to horizontal. This method was observed to result in a horizontal granular bed with a packing fraction ≈ 0.60. A minimum $Q = 50\ \mathrm{cm^3\,min^{-1}}$ was applied to create a uniform gap of the order of a few grain diameters between the top plate of the channel and the granular bed. The flow was then increased in steps to reach a desired Q value.

TABLE I. List of materials used in the experiments and their physical properties. The dispersion corresponds to the percentage difference between the maximum and minimum grain size and the mean grain size.

Material	d (μm)	Dispersion (%)	Material	Shape	ϕ_m (deg)
G-1	375 ± 25	6	Glass	Spherical	24
G-2	470 ± 38	8	Glass	Spherical	24
G-3	686 ± 25	4	Glass	Spherical	24
G-4	1060 ± 60	6	Glass	Spherical	24
Q-1	254 ± 43	17	Quartz	Angular	26

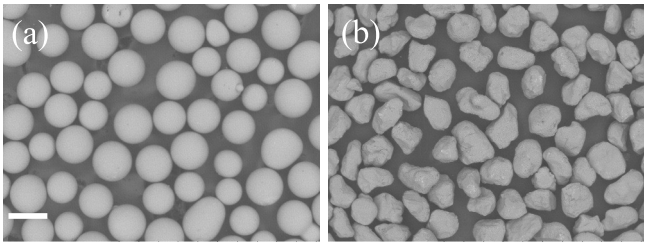

FIG. 2. SEM images of (a) glass beads (G-1) and (b) silica grains (Q-1) used in the experiments. The white scale bar corresponds to 400 μm in both images.

A 532 nm wavelength laser sheet is positioned perpendicular to the flow direction and is used to illuminate the dye in the fluid which then fluoresces. We focused on a location a few centimeters away from the mesh to ensure that it was unaffected by the flow transition from the pipe near the entrance to the channel. A digital camera with a resolution of 1040×1039 pixels is positioned to image the horizontal cross section of the granular bed. An optical high pass filter allows only light from the fluorescent dye to reach the camera, which makes it easier to identify the surface of the granular bed because the dye does not penetrate the glass beads. A sample image used to determine the bed height is shown in Fig. 1(b) and corresponds to the central half of the channel width to avoid direct influence of the side walls.

We obtain the height of the fluid h_f inside the channel by identifying the surface of the bed and measuring the height to the top plate of the channel (see Fig. 1(b)). To automate the measurement of the surface, we obtain an integrated intensity over a width of 8 mm corresponding to at least eight particles or more at the center of the channel as a function of height. The granular bed surface is observed to be flat to within a grain diameter in this location away from the side walls. This intensity is observed to decrease rapidly from the top of granular bed, and we use the point where the rate of decrease is greatest to identify the surface systematically. When comparing to the images directly, this point is found to be about 1/10–1/28 of a grain diameter from where a bead surface is first encountered. We thus assume that the point identified corresponds practically to the top of the bed surface. We have used other criteria—including one corresponding to the average height—and found it to give very similar trends for h_f reported and within the fluctuations from run to run.

The flow near the surface of a granular bed composed of similar spherical beads has been visualized by Goharzadeh *et al.*[18] using a refractive index matching technique. They found that the flow decays rapidly into the bed over a scale which is of the order of the diameter of the grains in the bed, where the interface was defined as the top edge of the highest grain at the interface. An exponential form is expected for a Brinkman-like interface layer[19] between a fluid and a porous bed. We have fitted their data using

$$v_x(y) = v_s \exp(y/l_b), \tag{3}$$

where v_x is the average velocity of the fluid parallel to the surface, v_s is the velocity at the surface, y is the distance from the bed surface, and $l_b \sim d/4$ is associated with length scale over which the flow is observed to decay. From Fig. 3(a), it can be seen that this form describes their data reasonably well. Then, by taking the derivative of Eq. (3) with respect to y and equating it to the shear rate at the bed surface $\dot{\gamma}$, and assuming continuity of the fluid flow, we can deduce that

$$v_s \approx \dot{\gamma} l_b. \tag{4}$$

It may be noted that this relation is similar to that proposed by Beavers and Joseph[20] for beds with relatively high porosity. Because the flow in the porous interface decays so rapidly inside the bed, its contribution to the net flow in the pipe is expected to be negligible. Therefore, we next calculate the flow of the fluid inside the channel assuming no-slip boundary conditions at the interface.

In the case of laminar flow in a rectangular pipe, the flow profile and the shear rate as a function of the pipe dimensions and the flow rate have been derived by Cornish.[21] We assume that the origin of the coordinate system is located on the surface of the granular bed at the center of the cross

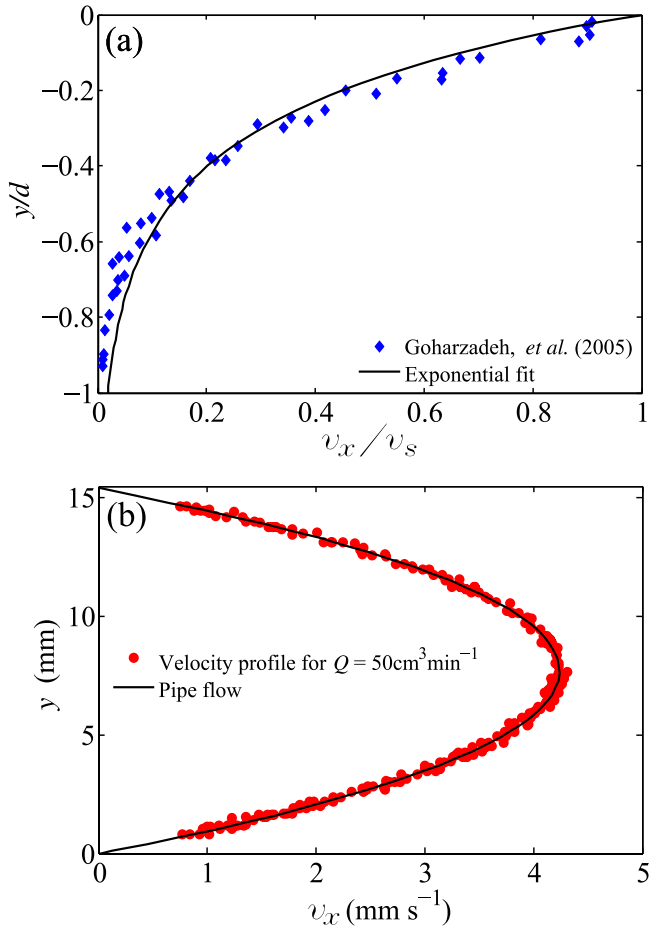

FIG. 3. (a) The average horizontal fluid velocity v_x along the flow direction as a function of depth inside the bed reported by Goharzadeh *et al.*[18] is fitted to Eq. (3) with $l_b = d/4$. (b) v_x as a function of height above the granular bed is compared with Eq. (5) for $z = 0$ cm.

section of the channel, and the x-axis is along the flow direction, the y-axis is oriented along the vertical and perpendicular to the surface, and the z-axis is perpendicular to the flow and parallel to the surface. Then, the velocity along the flow direction v_x is given by

$$v_x = -\frac{1}{2\mu}\frac{dp}{dx}\left(hy - y^2 - \frac{8h^2}{\pi^3}\left\{\frac{\cosh(\pi z/h)}{\cosh(\pi w/2h)}\sin\frac{\pi y}{h}\right\}\right), \tag{5}$$

where p is the pressure and h is the height of the channel. Higher order correction terms due to the side walls were calculated to be two orders of magnitude smaller and therefore ignored.

In order to check if this velocity equation works in our geometry, we measured the velocity profile using a standard Particle Imaging Velocimetry (PIV) technique for $Q = 50$ cm^3 min^{-1}. The measured velocity in the flow direction as a function of height above the granular bed is plotted in Fig. 3(b), along with the velocity profile for $x = 0$ in Eq. (5). We observe good agreement, confirming that the flow inside the bed makes negligible contribution to the overall flow. While we are unable to measure the flow quantitatively for higher flow rate, we checked that the flow remains laminar over the entire range of flow rates from observations that the tracer particles leave linear tracks parallel to the flow direction. This is also consistent with the fact that the maximum flow Re corresponding to the highest Q used in our experiments is around 10, which is well below the onset of instabilities in pipe flow.

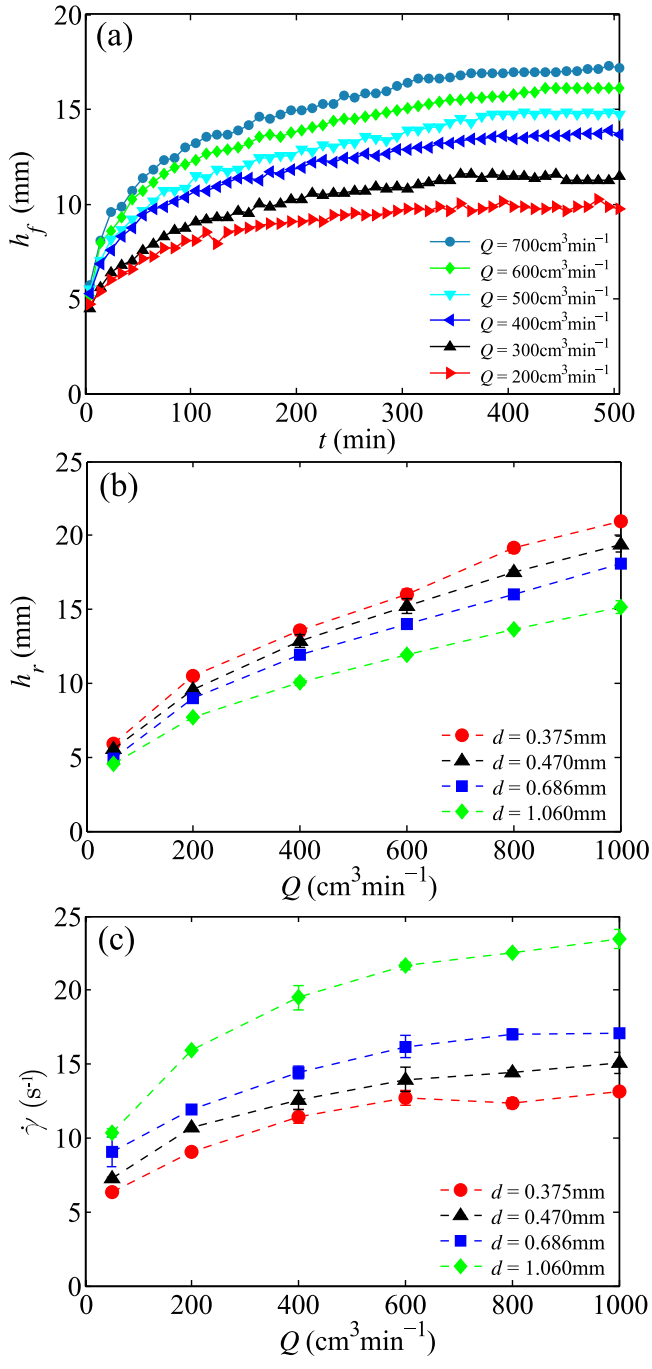

FIG. 4. (a) The height of the fluid h_f above the granular bed as a function of time t for various imposed flow rates Q ($d = 0.375$ mm). (b) The rest height of the bed h_r is observed to increase systematically with Q for each of the granular materials studied. (c) The shear rate at the threshold for erosion obtained from the measured h_r as a function of Q. The shear rate at threshold is observed to increase before approaching a constant value, indicating armoring of the bed. The error bars correspond to the standard deviation calculated using the 5 data sets obtained for each condition.

III. EVOLUTION OF THE BED HEIGHT AND ARMORING

We now discuss the measured height of the bed as a function of flow rate Q, and use it to deduce the critical shear rate at threshold. Figure 4(a) shows the evolution of the height of the fluid h_f in a typical run for various imposed Q. One observes that h_f increases rapidly and then slowly

approaches a rest height h_r corresponding to each applied Q. Examining the granular surface, we noted that erosion ceases when the height becomes constant. We found that bed erosion occurred when Q was then increased by the smallest increment available to us. Thus, the threshold value obtained by approaching the threshold from above is similar to that for onset of erosion. Further, plots of the measured h_r versus Q are shown in Fig. 4(b). The data shown are obtained by averaging over a time interval from 24 000 to 30 000 s when the rest height appears to reach a constant value, and further averaged over five experimental runs. The error bar corresponding to the standard deviation, obtained using the five data sets, can be noted to be of the order of the size of the symbols used to plot the data or smaller. These plots clearly show that h_r increases with Q and decreases with grain diameter.

To quantify the trends, we obtain the shear rate at the granular surface from Eq. (5) by taking its derivative with respect to y for $h = h_r$ and $y = 0$, which gives us

$$\dot{\gamma} = \frac{6Q}{wh_r^2} \cdot \left(\frac{1 - \frac{8}{\pi^2} \cdot \mathrm{sech}(\pi w/2h_r)}{1 - \frac{192h_r}{\pi^5 w} \cdot \tanh(\pi w/2h_r)} \right). \tag{6}$$

Now, a weak span wise dependence of the shear rate can be also noted in the central section of the channel by taking the appropriate gradient of Eq. (5). This systematic variation is found to increase from 0.5% to 5% as the cross section height increases with Q to the maximum value investigated. However, because the height of the bed is observed to be constant within a grain diameter, we assume that the resulting shear rate is essentially constant in the region over which we carry out measurements away from the side wall. This estimated $\dot{\gamma}$ is plotted as a function of Q in Fig. 4(c) for the granular beds with various d. One can observe that $\dot{\gamma}$ increases rapidly with Q before slowly approaching a constant value corresponding to each d. Because any lift force (shear lift or Bernoulli lift) is expected to lead to a reduction of normal stress at the interface, this would imply a lowering of $\dot{\gamma}$ at threshold. However, because we observe an increase in $\dot{\gamma}$ at threshold, we attribute the increase to armoring of the bed.

Armoring can arise because of many reasons, including preferential erosion of small particles in polydisperse beds which leaves behind harder to erode larger particles that then shield the bed below. Because the granular beds used in our study are essentially monodisperse (see Table I), this is not the reason for the observed armoring. We believe the observed armoring is in fact consistent with the armoring observed by Charru *et al.*[9] with monodisperse beads. They have noted that a freshly sedimented bed undergoes armoring when sheared over prolonged periods in an annular channel in which the grains do not leave the system. The shearing was observed to lead to consolidation of the bed as measured by the height of the bed. Because we are unable to directly measure the evolution of the volume fraction near the surface, we simply refer to the bed with the higher $\dot{\gamma}$ as armored in the discussion henceforth.

IV. PARTICLE REYNOLDS NUMBER AND LIFT FORCE

As noted in the Introduction, the magnitude of the drag and shear forces depends on the Reynolds number. Accordingly, we calculate Re_p from Eq. (2) with v_s estimated from Eq. (4) for each of the grain diameters. The calculated Re_p is then plotted in Fig. 5(a) over the range of Q used in our experiments. It is clear that Re_p is at least an order of magnitude less than 1, indicating that we are well within the low Reynolds linear regime for calculation of drag.

We next consider the importance of shear lift force over the Reynolds numbers in our experiments. It is well known that a stationary particle in a viscous shear flow will experience a lift.[22] While the shear lift force for a particle at the surface of a porous granular bed has not been calculated, Leighton and Acrivos[23] have calculated the shear lift force experienced by a stationary particle in contact with a wall under low Re conditions. They find a shear lift force given by

$$F_l = 0.57\, \rho_f v_s d^3 \dot{\gamma}. \tag{7}$$

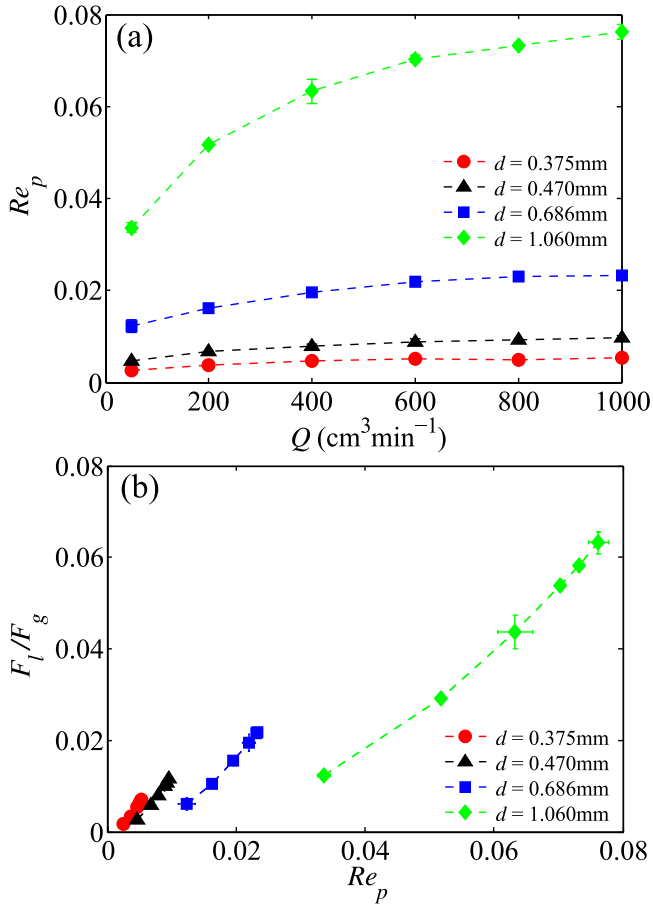

FIG. 5. (a) The particle Reynolds number Re_p as a function of Q. (b) The ratio of F_l and F_g for a sphere attached to a wall in a linear shear flow is observed to be well below one over the range of Re_p investigated in the experiments. The error bars correspond to the standard deviation calculated using the five data sets obtained for each condition.

Now, the difference of the gravitational force and buoyancy acting on a grain is given by

$$F_g = \frac{\pi}{6}(\rho_g - \rho_f)gd^3. \tag{8}$$

Therefore, to estimate the relative contribution of the shear lift force, we plot the ratio

$$\frac{F_l}{F_g} = \frac{1.09v_s\dot{\gamma}}{(\rho_g/\rho_f - 1)g} \tag{9}$$

in Fig. 5(b). The values indicate that the lift force is small compared to gravitational forces for the range of Re_p observed in the experiments in the case of a sphere attached to a planar wall experiencing a linear shear flow. Further, simulations[14] appear to show that the shear lift force decreases rapidly compared to the drag force, when the surface coverage of spheres on a surface is large. For these reasons, it appears that shear lift force can be expected to be negligible over the range of the Re_p investigated in our experiments.

V. CRITICAL SHIELDS NUMBER

We now obtain θ_c in order to compare our data to those discussed in the Introduction. It should be emphasized that ideally τ_d should include factors due to the geometry of the flow near the grains. However, for consistency with previous reports, we ignore this geometric effect in estimating θ_c. As discussed in Sec. IV, the ratio of F_l/F_g is negligible in the regime investigated in our experiments.

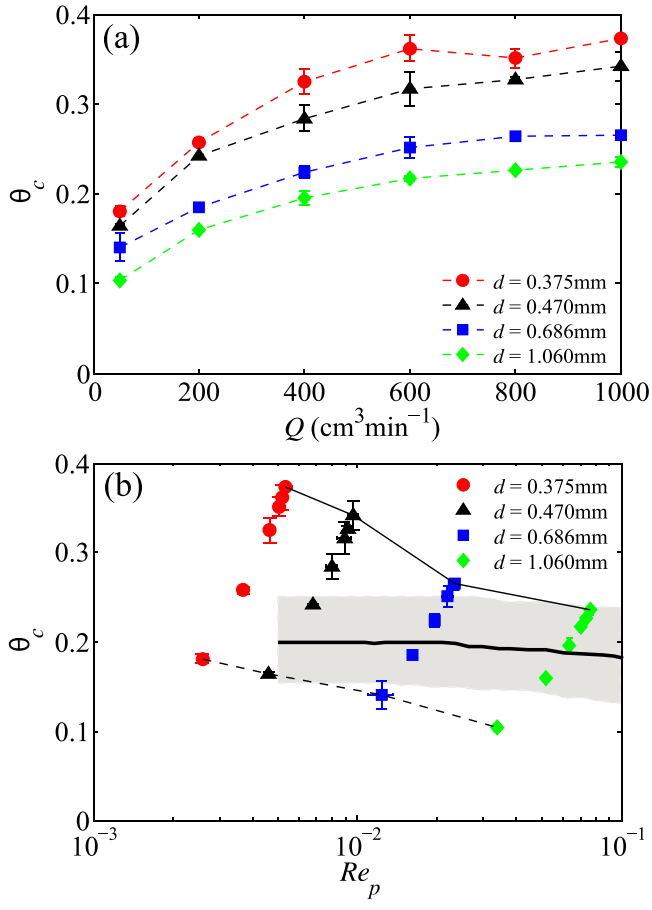

FIG. 6. (a) θ_c is observed to increase, and then approach a constant for each grain size due to the armoring of the bed. (b) θ_c is observed to decrease systematically for the freshly sedimented bed as well as the fully armored bed, which are indicated by the dashed and solid lines, respectively. The thick solid line represents the Shields curve and the approximate range of scatter is indicated by gray shading.[1,2] θ_c is expected to be constant over this range of Re_p.[13] The error bars correspond to the standard deviation calculated using the five data sets obtained for each condition.

Therefore, the shear stress is assumed to be given by $\tau_d = \mu\dot{\gamma}d^2$, $\sigma_g = (\rho_g - \rho_f)gd^3$. We then obtain

$$\theta_c = \frac{\mu\dot{\gamma}}{(\rho_g - \rho_f)gd} \tag{10}$$

which is plotted as a function of Q in Fig. 6(a). These plots clearly show that θ_c increases and saturates with Q, reflecting the effect of armoring seen in $\dot{\gamma}$. Further, one observes that θ_c approximately doubles for the fully armored case compared to when the bed is freshly prepared by sedimentation. Thus, θ_c over a wide range can be observed depending on bed preparation. While we can observe the bed surface (a sample image is shown in Fig. 1(b)), we cannot determine if the local packing or the relative height distribution of the grains at the surface changes to give rise to the armoring from such images.

We have also plotted θ_c versus Re_p in Fig. 6(b) as is often shown in the literature.[1,2,11] The effect of bed armoring is to lead to a locus of points for each grain size which fall on a line with a slope given by the ratio $\mu^2 d/\rho_f(\rho_g - \rho_f)g$. This systematic linear behavior is simply a consequence of the linear dependence of θ_c and Re_p on $\dot{\gamma}$, which are calculated from Eq. (10), and Eq. (2), and Eq. (4), respectively. One can further note that θ_c clearly decreases systematically for both the freshly sedimented bed as well as for the fully armored bed. In comparing the data to the Shields curve reported in the literature, we find that θ_c decreases in a regime where it is reported to be constant.[11,13] (The decreasing trend in the Shields curve was previously only clearly noted for Re_p

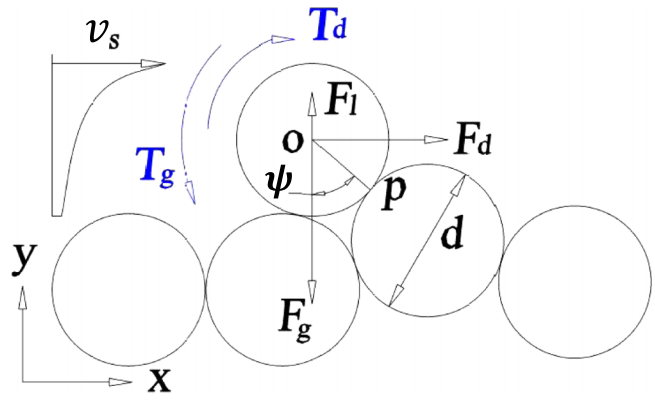

FIG. 7. The forces due to gravity F_g, drag F_d, and lift F_l effectively acting on the grain center. The torques acting on a grain on the granular surface at the threshold of motion about a pivot point P.

about 1–10.) Further, the observed values after the bed is armored are consistently greater than many recent studies in the laminar regime discussed in the Introduction.

VI. DISCUSSION OF THE STABILITY CRITERIA AT THRESHOLD

To understand the stability of the grain at the threshold of motion, we now discuss the torque balance about a pivot point P which subtends an angle ψ with the vertical as indicated in Fig. 7. Neglecting the torque exerted by shear lift force as per the discussion in Sec. IV,

$$T_d + T_g = 0, \tag{11}$$

where T_d is the torque because of the viscous drag due to the flow around the sphere and T_g is the torque due to gravitational force. Because F_g acts on the center of the sphere, the torque about the pivot point is given by

$$T_g = \frac{\pi}{12}(\rho_g - \rho_f) g d^4 \sin(\psi). \tag{12}$$

In case of the torque due to drag, it is to be emphasized that T_d is not simply given by the total drag force F_d times the perpendicular distance to the pivot point P, because of the further contribution of the torque imposed by the shear flow about the center.[16] An analytical form for the force and torque acting on a sphere in an exponentially decaying flow field is not available. However, we can use the stability condition in Eq. (11) to effectively measure this torque

$$T_d^m = -T_g,$$

for a given ψ.

In order to have a reference, we consider the torque acting on a sphere attached to a wall in a linear shear flow for which the drag force and torque about its center have been calculated by O'Neill.[24] Then, the torque acting on a sphere about the pivot point P is given by

$$T_d^f = 5.1\pi\mu\dot{\gamma}(d/2)^3 + 3.776\pi\mu\dot{\gamma}(d/2)^3\cos(\psi), \tag{13}$$

where $\dot{\gamma}$ corresponds to Eq. (6). We plot the ratio T_d^m/T_d^f as a function of ψ from 0 to 90° for each of the grain sizes in Figs. 8(a) and 8(b) for the freshly sedimented bed and the armored bed, respectively. It can be noted that T_d^m/T_d^f are overall similar but also systematically different from each other for the various d. Because the flow decays exponentially into the bed, one can expect T_d^f to be significantly greater than the actual torque due to drag. Further, in the analysis of a grain on a rough surface, Lee and Balachandar[16] used the angle of repose of the grains as ψ. We have measured a maximum angle of stability ϕ_m for the materials used in the experiments to be 24° in case of all the spherical particles. We can observe that T_d^m/T_d^f is well below one for a wide range of ψ around

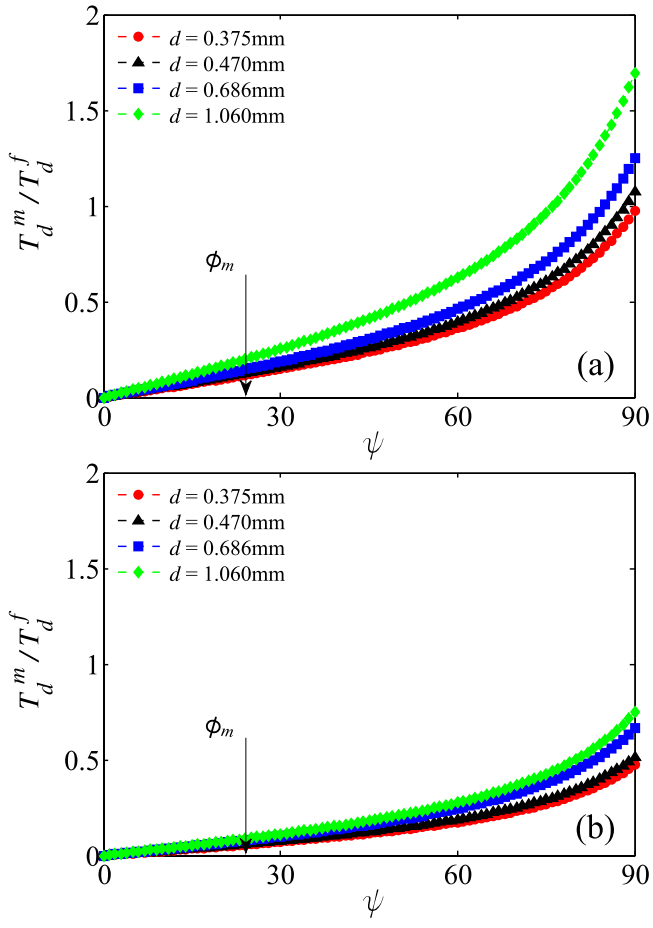

FIG. 8. The ratio T_d^m/T_d^f versus ψ for various granular materials investigated (a) $Q = 50$ cm^3 min^{-1} and (b) $Q = 1000$ cm^3 min^{-1} corresponding to freshly prepared and armored bed, respectively. Here, the normalization T_d^f corresponds to a sphere attached to a wall which is in a linear shear flow. The corresponding value of ϕ_m is also indicated.

ϕ_m, and lower for $\psi < \phi_m$. Thus, we conclude that the torques acting to dislodging the grains at the granular surface are significantly lower than that for a sphere about a similar pivot point which is fully exposed to a linear shear flow. This observation is consistent with the experiments by Fenton and Abbott which showed sensitive dependence of Shields number on the degree of protrusion,[25] and simulations of Derksen and Larsen[14] who found the shear forces are significantly affected by the amount of surface coverage, and the observation of rapidly decaying fluid flow near the granular surface by Goharzadeh *et al.*[18] However, because we do not have access to the detailed surface packing and its changes as the bed erodes, we are unable to further analyze the forces acting on the grains to understand the observed values in this study.

VII. EFFECT OF PARTICLE ROUGHNESS

To show that the trends observed were not particular to smooth spherical or glass grains, we now discuss data obtained using the quartz grains listed in Table I. By repeating the same procedure employed in the case of spherical grains, we obtained $\dot{\gamma}$ by measuring h_r with rough particles as a function of Q as shown in Fig. 9(a). As in the smooth case, we find that $\dot{\gamma}$ increases with Q, indicating an armoring of the bed. Because the quartz grains are even smaller compared to the spherical grains, shear lift force is considered to be even smaller. Thus, θ_c can be estimated to increase from 0.10 to 0.38 over the range of Re_p from 2.5×10^{-3} to 7.6×10^{-2}. These trends are similar compared

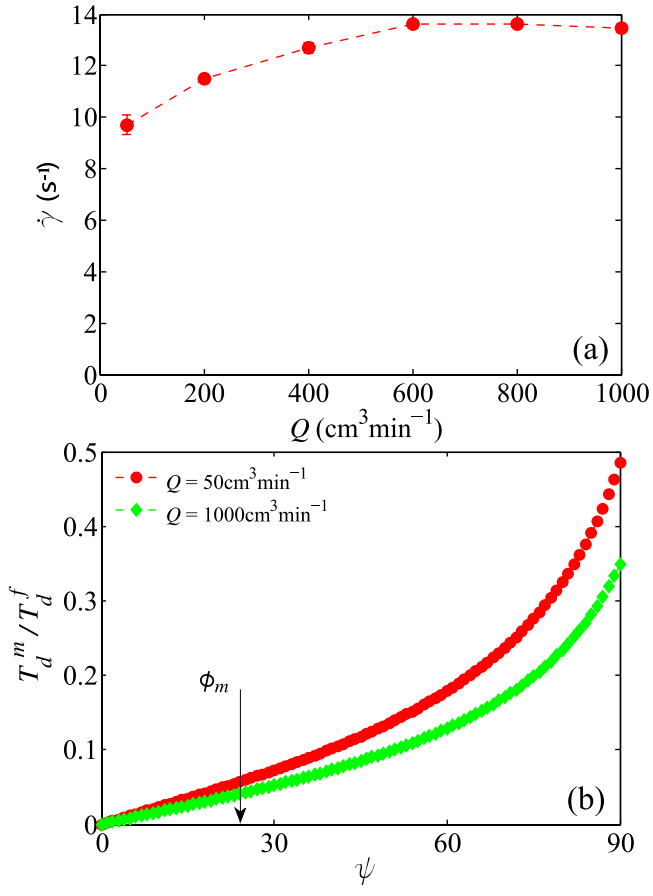

FIG. 9. (a) The shear strain at threshold for the quartz grains (Q-1) versus flow rate shows armoring. The error bars correspond to the standard deviation calculated using the five data sets obtained for each condition. (b) T_d^m/T_d^f versus ψ is well below one.

to the smooth spherical grains, except that values of θ_c are even higher. These higher values of θ_c are in line with the overall trend that θ_c increases with decreasing d as observed with the spherical grains. We have further estimated the ratio T_d^m/T_d^f for the rough quartz grains in Fig. 9(b). We find the ratio significantly smaller than one, indicating that the observed trends are not very sensitive to the roughness of the grains.

VIII. CONCLUSIONS

In conclusion, we have investigated the erosion threshold of a granular bed under laminar flow conditions and found significant effects of bed armoring and grain size dependence. In particular, bed armoring is observed to give rise to a systematic variation of critical Shields number with particle Reynolds number depending on whether the bed is freshly prepared or sheared over a prolonged period by bed load. Further, our data show that a wide range of critical Shields numbers are obtained with the same grains under similar flow conditions but with different bed preparations. Because the beds are composed of grains with a narrow grain size, the source of the armoring may have to do with the relative rearrangement of the grains at the surface rather than the armoring resulting from size sorting which is observed to lead to pavement formation in river beds.[26] However, because we are unable to visualize the packing into the bed, we are unable to provide direct data on the nature of the rearrangements in this study and how it may affect the flow near the bed interface.

Further, we have analyzed our data in terms of torque balance condition for threshold of motion, which has been noted[16] to give a lower threshold for motion compared with force balance

condition as captured by the critical Shields number. By analyzing the torque condition for stability, we find evidence that the estimated torque acting to dislodge grains at the bed surface is significantly lower than that acting on a sphere fully exposed to a linear shear flow. This strongly suggests that the grains at the bed surface are only partially exposed to flow, consistent with a previous study of the effect of degree of protrusion on the critical Shields number.[25] The pivot point has been taken to be given by the angle of repose from the vertical in numerical study of onset of motion of a single particle in a shear flow.[16] In case of the spherical grains, we obtain the same maximum angle of stability for all the grain sizes (which is similar to the angle of repose). However, we observe that the ratio of the measured torque relative to the torque experienced by a sphere fully exposed to a linear shear flow does not collapse on to a single curve (see Fig. 8). This suggests that the pivot point is different than that given by the maximum angle of stability and grain size dependent. Thus, in order to fully estimate the torque, further measurements of the typical pivot points for the motion of the grains at threshold are needed.

Finally, our study with rough quartz grains–which is also more typical of natural materials–finds over-all trends on armoring to be consistent with those for smooth spherical particles showing the generality of our results. The measured maximum angle of stability of these grains is somewhat higher than that for spherical grains, but the critical Shields number is found to be significantly higher. This higher value is, however, consistent with the overall trend observed that smaller grain size yields a higher critical Shields number. Further visualization of the physical evolution of the bed is necessary to develop a deeper understanding of the armoring and observed grain size dependence of the erosion threshold.

ACKNOWLEDGMENTS

We thank Vikrant Yadav and Ashish Orpe for help with experiments and David Johnson for discussions. Anyu Hong thanks the Department of Physics at Clark University for its hospitality while this work was conducted and acknowledges the support of the Chinese Scholarship Council. This material is based upon work supported by the U.S. Department of Energy Office of Science and Office of Basic Energy Sciences program under DE-FG02-13ER16401.

[1] A. Shields, "Anwendung der Ähnlichkeitsmechanik und der Turbulenz-forschung auf die Geschiebebewegung," Preussische Versuchsanstalt für Wasserbau und Schiffbau Report No. 26, 1936.
[2] J. M. Buffington and D. R. Montgomery, "A systematic analysis of eight decades of incipient motion studies, with special reference to gravel bedded rivers," Water Resour. Res. **33**, 1993–2029, doi: 10.1029/96WR03190 (1997).
[3] L. C. Van Rijn, "Principles of sediment transport in rivers," in *Estuaries and Coastal Seas* (Aqua Publications, Amsterdam, 1993).
[4] M. S. Yalin and E. Karahan, "Inception of sediment transport," J. Hydraul. Div. **105**, 1433–1443 (1979), abstract available at http://cedb.asce.org/cgi/WWWdisplay.cgi?9113.
[5] M. Pilotti and G. Menduni, "Beginning of sediment transport of incoherent grains in shallow shear flows," J. Hydraul. Res. **39**, 115–124 (2001).
[6] P. A. Mantz, "Incipient transport of fine grains and flakes by fluids extended shield diagram," J. Hydraul. Div. **103**, 601-615 (1977), abstract available at http://cedb.asce.org/cgi/WWWdisplay.cgi?7413.
[7] S. J. White, "Plane bed thresholds of fine grained sediments," Nature **228**, 152–153 (1970).
[8] L. Malverti, E. Lajeunesse, and F. Métivier, "Small is beautiful: Upscaling from microscale laminar to natural turbulent rivers," J. Geophys. Res.: Earth Surf. **113**, F4, doi: 10.1029/2007JF000974 (2008).
[9] F. Charru, H. Mouilleron, and O. Eiff, "Erosion and deposition of particles on a bed sheared by a viscous flow," J. Fluid Mech. **519**, 55–80 (2004).
[10] T. Loiseleux, P. Gondret, M. Rabaud, and D. Doppler, "Onset of erosion and avalanche for an inclined granular bed sheared by a continuous laminar flow," Phys. Fluids **17**, 103304 (2005).
[11] M. Ouriemi, P. Aussillous, M. Medale, Y. Peysson, and E. Guazzelli, "Determination of the critical Shields number for particle erosion in laminar flow," Phys. Fluids **19**, 061706 (2007).
[12] A. E. Lobkovsky, A. Orpe, R. Molloy, A. Kudrolli, and D. Rothman, "Erosion of a granular bed driven by laminar fluid flow," J. Fluid Mech. **605**, 47–58 (2008).
[13] P. L. Wiberg and J. D. Smith, "Calculations of the critical shear stress for motion of uniform and heterogeneous sediments," Water Resour. Res. **23**, 1471–1480, doi: 10.1029/WR023i008p01471 (1987).
[14] J. J. Derksen and R. A. Larsen, "Drag and lift forces on random assemblies of wall-attached spheres in low-Reynolds-number shear flow," J. Fluid Mech. **673**, 548–573 (2011).
[15] C. Chan-Braun, M. García-Villalba, and M. Uhlmann, "Force and torque acting on particles in a transitionally rough open-channel flow," J. Fluid Mech. **684**, 441–474 (2011).
[16] H. Lee and S. Balachandar, "Critical shear stress for incipient motion of a particle on a rough bed," J. Geophys. Res.: Earth Surf. **117**, F1, doi: 10.1029/2011jf002208 (2012).

[17] P. Dontula, C. W. Macosko, and L. E. Scriven, "Does the viscosity of glycerin fall at high shear rates?," Ind. Eng. Chem. Res. **38**, 1729–1735 (1999).
[18] A. Goharzadeh, A. Khalili, and B. B. Jørgensen, "Transition layer thickness at a fluid-porous interface," Phys. Fluids **17**, 057102 (2005).
[19] H. C. Brinkman, "A calculation of the viscous force exerted by a flowing fluid on a dense swarm of particles," Appl. Sci. Res. A **1**, 27–34 (1947).
[20] G. S. Beavers and D. D. Joseph, "Boundary conditions at a naturally permeable wall," J. Fluid Mech. **30**, 197–207 (1967).
[21] R. J. Cornish, "Flow in a pipe of rectangular cross-section," Proc. R. Soc. London **120**, 691–700 (1928).
[22] P. G. Saffman, "The lift on a small sphere in a slow shear flow," J. Fluid Mech. **22**, 385–400 (1965).
[23] D. Leighton and A. Acrivos, "The lift on a small sphere touching a plane in the presence of a simple shear flow," Z. Angew. Math. Phys. **36**, 174–178 (1985).
[24] M. E. O'Neill, "A sphere in contact with a plane wall in a slow linear shear flow," Chem. Eng. Sci. **23**, 1293–1298 (1968).
[25] J. D. Fenton and J. E. Abbott, "Initial movement of grains on a stream bed: The effect of relative protrusion," Proc. R. Soc. A **352**, 523–537 (1977).
[26] G. Parker and P. C. Klingeman, "On why gravel bed streams are paved," Water Resour. Res. **18**, 1409–1423, doi: 10.1029/WR018i005p01409 (1982), 1982.